NACA

RESEARCH MEMORANDUM

PRELIMINARY EVALUATION OF THE WING LEADING EDGE AS A MISSILE-MOUNTING LOCATION

By P. R. Hill and S. Hoffman

Langley Aeronautical Laboratory
Langley Field, Va.

NATIONAL ADVISORY COMMITTEE
FOR AERONAUTICS

WASHINGTON
January 16, 1957

NATIONAL ADVISORY COMMITTEE FOR AERONAUTICS

RESEARCH MEMORANDUM

PRELIMINARY EVALUATION OF THE WING LEADING EDGE AS A MISSILE-MOUNTING LOCATION

By P. R. Hill and S. Hoffman

SUMMARY

Rocket-model flight tests and full-scale launching tests were made to evaluate some of the major aspects of mounting and launching missiles from the leading edge of a wing. Zero-lift drag tests were made of an airplane model having wings with 45° of sweep, an aspect ratio of 4, and an NACA 65A004 section. Six missile models were mounted on the wing leading edge in two tests and on struts in a contemporary underwing position in another test. A Mach number range from 0.8 to 1.3 was covered.

For a range of Mach number from 1.1 to 1.3, the drag from the leading-edge missile installation was less than the drag of six isolated missiles. The underwing installation tested had a drag increment about 50 percent greater than this amount over the corresponding speed range. The subsonic drag increment of the leading-edge mounted missile was unfavorable but small.

Full-scale launching tests of a missile from the leading edge of a wing mock-up showed that the blast damage to the wing was superficial. The rise in temperature of the wing structure was negligible. The rocket internal ballistics were somewhat altered during the early phase of burning and the initial missile acceleration was greatly augmented.

INTRODUCTION

Some aspects are presented of the use of the airplane leading edge as a missile-mounting and missile-launching location. The objectives of the use of the wing leading edge for launching missiles are to utilize a location that is accessible and convenient, has an uninterrupted view of targets which may be "locked on" before release, is a fairly simple installation, and has a favorable interference drag with the wing.

Favorable pressure interference results from the back of the missile riding in the positive pressure field of the wing leading edge. This tends to push the missile forward and compensates for part of the pressure drag at the forward end of the missile. The existence of such a pressure field and its favorable effects is clearly demonstrated in reference 1. The effect of the rocket blast on the wing during the launching phase is an item requiring investigation, however, and is possibly the reason that this location has not been given much study. A preliminary investigation of some of the main considerations such as the drag of a wing-leading-edge mounted missile and of the rocket-blast effects on a wing leading edge are described in this paper.

The Langley Pilotless Aircraft Research Division (PARD) has had a number of years of experience in launching many types of rockets from many types of launchers. This experience has generally indicated that the direct blast effects such as erosion and heating are very much less than would be expected since the duration of high-intensity exposure for typical high-acceleration vehicles is of the order of 0.05 second. Rather comprehensive experience has also been obtained in launching rockets locked together in tandem. PARD has established the practice of securing two rocket stages together by use of a male adapter or nozzle fitting that fits into the nozzle of the forward rocket motor. Such an adapter is shown (see fig. 1) fitted into a cutaway nozzle of a $3\frac{1}{4}$-inch aircraft rocket for which it forms a rigid mount. Further information concerning this method of mounting is given in reference 2. In consideration of the drag after launching, it should be noted that the male adapter can be made to conform closely to a streamline shape. It appears, therefore, that a nozzle adapter would also be a suitable mounting device and launching fitting for missiles on the leading edge of a wing.

Since this paper amounts to a proposal of a missile-mounting location, it seems in order to express some thoughts on possible applications. The missile installation on the wing leading edge could be used on any airplane on which forward firing rockets can be employed. This could be on conventional fighter or interceptor airplanes, on tactical airplanes, or even on bombers. Current thinking on the defense against the conventional turbojet or turboprop bomber is shifting toward the consideration of much larger bomber-destroying or bomber-destroyer airplanes than those employed at the present time. This is based on the ability of the larger airplane to carry a greater missile load and effectively engage the enemy farther from the defended positions. As already mentioned, one of the principal features of the wing-leading-edge mounting is the expected favorable interference drag. The amount of interference would naturally depend, among other things, on the relative size of the missile and the airplane. The ratio of missile length to mean wing chord, which might be taken as a measure of relative size, is 0.655 for the present tests.

This is roughly comparable to a Hughes Falcon missile mounted on current interceptors. The relative size of the missiles and the larger destroyer airplanes will be determined by some of their principal requirements which are listed very briefly: (1) sufficient size and radius of action to establish defense in depth, (2) missile size and speed sufficient to outrange the attackers' defending missiles, and (3) airplane speed greater than that of the attacker.

If the destroyer airplane were to have double the (wing) dimensions of a present-day interceptor, and if the interceptor missiles it carried had twice the dimensions of the Falcon, they would, of course, bear the same ratio of missile size to airplane size as that of the models tested. Such increases in size are in conformity with items 1 and 2 for it is well known that a large airplane has longer range than a small one and, on the other hand, the larger missile, having about twice the weight-to-drag ratio, should have about twice the range of the smaller version. Hence, the ratio of the missile length to wing chord of the present tests is at least of the right order of magnitude to apply to this case, also.

The optimum location for mounting or storing missiles naturally depends on the purpose and on so many other factors that categorical statements cannot be made. One such factor that can enter, especially when the urgency of defense is great, is that of obtaining a system which is relatively simple and interferes little with space usually allotted for other functions. Hence, such a system lends itself to adaptation to airplanes already designed or built with the aim of reducing conversion lead time.

SYMBOLS

A	cross-sectional area, sq in.
a	tangential acceleration, ft/sec^2
C_D	total drag coefficient, based on S_w
C_{D_F}	missile drag coefficient, based on S_F
C_{D_f}	friction drag coefficient, based on S_w or S_F
g	acceleration due to gravity, 32.2 ft/sec^2
L	length of fuselage, in.
l	length of missile, in.

[redacted]

M	free-stream Mach number
q	free-stream dynamic pressure, lb/sq ft
R	free-stream Reynolds number based on wing mean aerodynamic chord
S_W	total plan-form area of wing, sq ft
S_F	maximum cross-sectional area of missile body, sq ft
W	weight of model, lb
X	station measured from nose of basic wing-body configuration, in.
x	station measured from nose of missile, in.
γ	angle between flight path and horizontal, deg

MODELS

Flight Models

Details and dimensions of the four zero-lift, free-flight models tested are given in figures 2 to 4 and tables I to IV. Photographs and the normal cross-sectional-area distributions of the configurations are presented in figures 5 and 6, respectively.

The basic configuration, model A, consisted of a sweptback wing and parabolic fuselage with two sweptback stabilizing fins in the vertical plane. The wing had a sweepback angle of 45° along the quarter-chord line, an aspect ratio of 4.0 (based on total wing plan-form area), a taper ratio of 0.6, and an NACA 65A004 airfoil section parallel to the free-stream direction. The fuselage was formed from two parabolas of revolution joined at the maximum diameter station (40 percent of body length) and had an overall fineness ratio of 12.5. The ratio of total wing plan-form area to fuselage frontal area was 25.8. Except for the steel fuselage noses, the models were constructed entirely of aluminum alloys.

Figure 3 gives the details and dimensions of the air-to-air missile configurations utilized in the tests. The missile configuration was selected to simulate a present-day airborne missile. The ratio of missile-body frontal area of six missiles to total wing plan-form area was 0.00357.

[redacted]

Models B and C (fig. 4(a)) were duplicate configurations, each having six missiles mounted along the wing leading edge. Three missiles were mounted on each wing panel at stations corresponding to 30, 50, and 70 percent of the semispan. The leading-edge adapters used for mounting the missiles were designed to provide a smooth fairing from the missile afterbody to the wing maximum thickness.

Model D consisted of the basic configuration with six strut-mounted missiles located in underwing positions, but otherwise identical to the missiles mounted on models B and C. Three missiles were mounted on each panel but were located on opposite surfaces of the wing panels. (See fig. 5(b).) This asymmetric arrangement was selected on the premise that any trim change would produce roll rather than pitch and the model would fly at essentially zero lift. For the vertical positioning of the missiles, the minimum distance between the missile body surface and wing surface was kept constant at 1.33 missile diameters. The chordwise locations were determined by alining the center of gravity of each missile with respect to the quarter-chord line of the wing. The spanwise stations were identical to those used for the leading-edge missiles. The airfoil section of the unswept struts used for the underwing installations had a flat-plate midsection, 15° wedges at the leading and trailing edges, and a thickness ratio of 0.068.

Blast-Investigation Equipment

For the blast investigation, a magnesium mock-up was made of the leading 20 percent of a 45° sweptback wing. The basic-wing airfoil section was an NACA 65(06)A007 of 10 feet total chord in the stream direction. It was constructed of 0.25-inch-magnesium sheet stock. A male-rocket-nozzle adapter of standard design of the Langley Pilotless Aircraft Research Division (PARD) was incorporated at the leading edge as a launching fitting. Details of the equipment are shown in figure 7. The adapter is screwed on the end of a structural tube that penetrates the wing and was welded to a spar located at the 20-percent station. In order to fasten easily the wing segment to the concrete launching apron, it was mounted with the leading edge perpendicular to the apron and the nozzle adapter or launching fitting inclined at 45° with the wing leading edge. (See fig. 8(a).)

The HVAR rocket motors used had a thrust of approximately 5,000 pounds, which is typical of the thrust of some air-to-air missiles, and, therefore, were deemed suitable for investigating blast effects. These motors had been modified by replacing the multiple-orifice standard nozzle by a single-orifice nozzle of the same total throat area. These motors were fitted with four stabilizing fins and with inert heads that brought the total launching weight to 122 pounds. Figure 8(a) shows the fin-stabilized rocket mounted on the wing segment ready for launching.

[redacted]

In these motors the igniters are located in the head end of the rockets. Standard igniters have metal powder cases which would probably cause an unnecessary degree of damage to the wing leading edge. These igniters were replaced by igniters with plastic cases. The furnishing of igniters with plastic cases is standard practice at PARD. The firing leads were brought out through the nozzle and into the launching fitting through a 5/8-inch-diameter hole in the tip of the launching fitting, then out through a vent hole in the bottom of the launcher. Figure 8(b) is a closser view showing the nozzle in place over the launching fitting. The nozzle used had a throat about 6 inches long, sometimes referred to as a high-pressure tail pipe, separating the motor from the expanding part of the nozzle. This is plainly visible in figure 8(b). Note that for these tests the top of the nozzle is within 2 inches of the wing leading edge at launching to maximize blast effects.

TESTS AND MEASUREMENTS

Flight Tests

All the models were tested at the Langley Pilotless Aircraft Research Station at Wallops Island, Va. All flight models were propelled from zero-length launchers by fin-stabilized booster rocket motors (fig. 5(c)) to supersonic speeds. After burnout of the rocket motors, the drag of the boosters and models separated and the models decelerated through the test Mach number range. Velocity and trajectory data were obtained from the CW Doppler velocimeter and NACA modified SCR-584 tracking radar, respectively. A survey of atmospheric conditions including winds aloft was made by rawinsonde measurements from an ascending balloon that was released at the time of each launching.

The flight tests covered continuous ranges of Mach numbers varying between Mach numbers of 0.8 and 1.32. The corresponding Reynolds numbers varied from approximately 2.8×10^6 to 5.9×10^6, based on wing mean aerodynamic chord. (See fig. 9.)

The values of total drag coefficient, based on total wing plan-form area, were obtained during decelerating flight with the expression

$$C_D = -\frac{W}{qgS_w}(a + g \sin \gamma)$$

where a was obtained by differentiating the velocity-time curve from the CW Doppler velocimeter. A more complete description of reducing the data is given in reference 3.

The probable error in total-drag coefficient was estimated to be less than ± 0.0007 at supersonic speeds and ± 0.001 at subsonic speeds. The Mach numbers were determined within ± 0.01 throughout the test range.

Launching Tests

The launching tests were of two types. In the first type, three fin-stabilized rockets were launched from the wing-leading-edge launcher described in the section entitled "Models." The tests made were very simple and mainly consisted of determining damage and approximate temperature rise by inspection before and after launching. However, a Fastax camera with timer was used to record the motion of the dummy missile leaving its launcher fitting. Following the first launch, the hole in the front of the launching fitting was enlarged to $1\frac{1}{8}$ inch in diameter to permit the firing leads to enter the adapter.

In the second type of launching test, the HVAR rocket motor was replaced by surplus JATO, 1.2-KS-4300, T42 rocket motors (ref. 4). The total weight and thrust of the simulated missiles remained about the same as those of the first vehicles used. Standard T42 igniters located in the nozzle throat were utilized. In this instance a pressure gage was attached to the rear end of the rocket case to measure the internal pressure, and a 50-foot trailing wire was used so that the maximum pressure reached during the launching phase could be recorded. Two tests were made. One utilized the wing-leading-edge launching fitting with the nozzle completely blocked. The other was made without a launcher by propping the motor up at the desired angle. No blockage of the nozzle occurred in this test other than that occasioned by the standard igniter itself.

RESULTS AND DISCUSSION

Flight Tests

Figure 10 presents basic drag data. The solid-line curves are fairings through the total C_D test points. The drag data of the basic model is shown in figure 10(a). Figure 10(b) gives the measured drag data for two identical flight models with six missiles mounted on the wing leading edge. The agreement is good and indicates the repeatability of the measurements. Figure 10(c) shows similar data for the under-wing mounted missiles.

The dashed curves give the computed skin friction using the equations of Van Driest (ref. 5). The flow over the fuselage was assumed turbulent because of the parting line between the steel-fuselage nose tip and the rest of the fuselage. The flow over the tail was assumed laminar up to the 50-percent-chord station. For the basic model with smooth metal wings, transition was assumed at the 40 percent chord. Agreement of calculated friction with the measured test drag at a Mach number of 0.8 can be noted. With the missiles mounted at the wing leading edge, the transition was assumed at 15 percent chord. Agreement with the measured subsonic drag is again obtained. With the missiles mounted underwing, transition was assumed at 40 percent chord on the upper surface and at 15 percent chord on the lower surface. About half of the difference in the friction curve and the observed subsonic drag can be accounted for by the missile-wing trailing edge and missile-body base drags. It seems reasonable that the remaining increment is due to the missile being immersed in the strong pressure field close to the wing.

Unpublished data shown in figure 11 give the total drag coefficient near zero lift of a single large-scale missile of the same configuration as those used in the present tests except for a sharper wing trailing edge. The lower drag for a sharper trailing edge was estimated (by use of ref. 6) to compensate for the increase in drag resulting from more extensive turbulent flow over the larger scale test. The data of figure 11 were, therefore, used directly as the reference isolated drag of the missile models. The dashed curve in figure 11 gives the estimated model friction drag.

Figure 12(a) shows a comparison of the total-drag coefficients of the configurations tested. The drag coefficient of six isolated missile models is also shown for comparison. The drag with the wing-leading-edge mounted missiles is everywhere less than the drag with the underwing-mounted missiles. At supersonic speeds, from Mach numbers of 1.1 to 1.3, the difference in drag of the basic model and the model with six missiles mounted on the leading edge is less than the drag of six isolated missiles. Near $M = 1.3$, the incremental drag from the leading-edge missiles is approximately half that of the isolated missiles. For a range of Mach number from 1.1 to 1.25, the average difference in drag of the basic model and the drag with six underwing-mounted missiles is about 50 percent greater than the drag of six isolated missiles.

Another result of the flight tests may be noted. At a Mach number of 0.8, the C_D of six isolated missiles from figure 12(a) is about 0.0013. The difference between the basic model and the models with six missiles on the leading edge is about 0.0023. The corresponding difference for the underwing-mounted missiles is about 0.0035. The differences between 0.0013 and the other values are, of course, unfavorable interference. The 0.0010 interference drag coefficient at this Mach number with the missiles mounted on the wing leading edge can be accounted for by assuming that the transition was moved far forward on the wing.

Of the 0.0022 interference drag coefficient on the model with missiles mounted in the underwing position, about 60 percent can be accounted for by exposed strut drag and a forward movement of transition on the lower surface of the wing; whereas the rest is pressure interference and errors. However, it is probable that transition on a basic full-scale airplane wing, particularly on the upper wing surface, would be farther ahead than on the model tests. It can, therefore, be inferred that the friction interference drag on a full-scale airplane may be somewhat less than that obtained on all the present model tests.

Figure 12(b) shows a comparison of the pressure drag coefficients of the configurations tested. These were obtained by subtracting the calculated friction drag coefficients from the total drag coefficients. A comparison of the pressure drag coefficients of the models with six missiles mounted on the leading edge with the basic configuration and six isolated missiles shows that the interference pressure drag is favorable at all Mach numbers above 1.0. The interference pressure drag is especially favorable above $M = 1.2$ where the pressure-drag increment due to the missile installation is negative. A similar comparison for the underwing-mounted missiles shows that the pressure-drag increment is a little greater than the pressure drag of the isolated missiles over most of the speed range tested. At transonic speeds, the results are in qualitative agreement with the concept of the transonic area rule, as may be seen by comparing the pressure drags (or drag rises) with the normal cross-sectional-area distributions of the models in figures 6(a) and 6(b). In brief, the area rule states that the zero-lift drag rise near the speed of sound is primarily dependent on the axial distribution of cross-sectional area normal to the axis of symmetry. The configuration with the strut-mounted underwing missiles (model D), which has the higher drag rise, has the greater maximum cross-sectional area and apparently the bumpier area distribution (fig. 6(b)). Area-rule analysis also suggests that the drag penalty due to the missiles in either of the positions investigated could be reduced markedly by use of less blunt missiles with a more favorable area distribution than the present one (fig. 6(c)).

In summary, the friction interference was unfavorable and the pressure interference was favorable for the model with six missiles mounted on the leading edge. The net result for this model at the supersonic speeds tested was a reduction in drag due to a thrusting force developed from favorable pressure interference. In contrast to this, the model with underwing-mounted missiles in locations which are typical of contemporary practice experienced unfavorable interference effects through most of the speed range. At subsonic speeds the interference drag coefficients were 0.0010 and 0.0022 for the leading edge and underwing mounting, respectively.

Launching Tests

Blast damage.- Figure 13(a) shows a photograph taken after the first launching from the same location as that in figure 8(b). No damage can be seen from this view. Figure 13(b) is a closer view showing some erosion of the nose of the duralumin launching fitting which fits into the nozzle throat. On the adapter or fitting shoulder can be seen some marks from the impact of the firing leads and a few pits made by igniter particles. The damage to the wing leading edge was very superficial. Approximately 4 inches of the leading edge above the launcher was lightly pitted from small particles which were undoubtedly small pieces of the plastic igniter. The slightly darkened leading edge in this area can be observed in figure 13(b). No other portion of the wing was damaged. The black line on the wing below the launcher fitting was some black insulation rubbed from the firing leads which were left hanging loose.

Two subsequent firings made after the hole in the top of the launcher filling was enlarged to $1\frac{1}{8}$ inches had no apparent effect on the wing. However, some further erosion of the launching fitting occurred. Figure 13(c) shows a view after three consecutive launchings. No additional firing lead prints were evident, showing that the leads had fired into the enlarged hole in the launcher fitting. Altogether, the total damage was superficial.

Temperature effects.- The ambient temperature and the temperature of the equipment at the time of firing was 55° F. A few seconds after firing, the temperature of the wing leading edge just above the launching fitting where the wing was closest to the rocket was about 100° to 110° F. The conical portion of the launcher fitting was estimated to be 140° F, whereas the temperature of the tip of the fitting was somewhat higher. No rise of temperature of the wing surfaces generally could be noticed. Because of the short duration of exposure, the rises in temperature of those parts of the wing which were exposed to the rocket jet appeared to be so low as to have no significance.

Launching speed.- The distance moved from the launching fitting as a function of time as determined from the Fastax camera records is shown in figure 14. In the same figure is shown the calculated distance moved based on test-stand thrust measurements of similar motors with no blockage of the nozzle. The indication is plain that a faster launching occurs from a fixed-nozzle plug than occurs from a free launch with unblocked nozzle. The fact that a missile launched in the vicinity of the wing, where the flow field deviates from the free-stream direction, remains in the distorted flow field a shorter time could be of practical significance in getting a clean launching. The observed fast launchings from this type of missile arise from two causes. First, of course, is a more rapid and greater buildup of internal pressure in the early phases

of burning. Second, and probably more significant, is the effects of the bow wave ahead of the nose of the nozzle adapter. Shortly after the nozzle clears the adapter, the Fastax films show a bow wave emerge from the nozzle and remain standing in front of the adapter nose. While the bow wave is in the nozzle, static pressures on the nozzle skirt probably reach values of over 1,000 lb/sq in. A marked rise in initial acceleration would, therefore, be expected.

In the particular case of a wing-leading-edge launched missile, the fact that the missile is already ahead of a considerable portion of the wing flow field when launched could be of further practical significance since the missile usually is required to negotiate the flow field near the wing with locked controls to avoid the possibility of a missile turning into the fuselage. Subsonic-flow-field angularities are graphically illustrated in figure 7 of reference 7 which shows that the flow angularity at zero and cruising lift coefficients is substantial in the vicinity of the leading edge but that the angularity rapidly decreases with distance forward of the leading edge. The downwash below the wing is substantial and influences missiles being launched from below the wing positions. An underwing-launched missile would pitch up below the wing and pitch down forward of the wing. Missiles fired from the leading edge would be expected to pitch down. However, the increased launching velocity should minimize the amount of pitch.

Internal ballistics.- The following discussion is relative to the tests made to check the rise in internal pressure by launching a T42 rocket motor (ref. 4) from the wing-leading-edge launcher fitting. The combination of the igniter and launcher fitting completely blocked the nozzle. This test showed a peak internal pressure of 1,790 lb/sq in. abs occurring during igniter burning. The pressure rose to this value in 0.043 second. The corresponding missile which was given a free launching had a peak pressure during igniter burning of 600 lb/sq in. abs occurring 0.045 second after initiation of ignition. The ignition characteristics of these particular motors were so slow that peak combustion pressures were not reached before the slack in the trailing wires over which the data were transmitted was used up. The greatest combustion pressure recorded was 1,575 lb/sq in. abs at 0.35 second on the freely launched missile, at which time the pressure was still rising but may have been near a maximum. One of the same batch of motors, fired on a static-thrust stand at an ambient temperature of 70° F, had a peak combustion pressure of 1,695 lb/sq in. abs. The igniter pressure with a blocked nozzle was of the order of 100 to 200 lb/sq in. higher than normal combustion pressure. Evidently, some adjustment of the amount of igniter powder used is indicated to keep the ignition peak below the maximum normal combustion pressure. However, the relatively small amount by which the maximum pressure was increased correlates well with PARD experience in many firings in which an adapter momentarily blocked the nozzle and the rocket cases were never exploded or ruptured.

CONCLUSIONS

Zero-lift aerodynamic drag tests were made of an airplane model having wings with 45° of sweep of the quarter-chord line, an aspect ratio of 4.0, and an NACA 65A004 airfoil section with six missile models mounted on the wing leading edge. The drag tests and full-scale launching tests of rocket vehicles from the leading edge of a mock-up wing led to the following conclusions:

1. At subsonic speeds the increase in model drag due to adding the missile models to the leading edge may be accounted for by a change in skin friction.

2. At supersonic speeds the favorable pressure interference from the leading-edge missiles was greater than the unfavorable friction interference so that the installation cost was less than total drag of the isolated missiles.

3. The blast damage to the wing leading edge and launcher was superficial.

4. The rise in wing temperature due to rocket blast was negligible.

5. Missiles launched from the leading-edge launching fitting, which blocked the rocket nozzles, accelerated more rapidly than missiles launched with unblocked nozzles.

6. Igniter peak pressure experienced with the blocked nozzle was of the order of 100 to 200 lb/sq in. greater than the normal combustion pressure.

Langley Aeronautical Laboratory,
National Advisory Committee for Aeronautics,
Langley Field, Va., September 25, 1956.

REFERENCES

1. Smith, Norman F., and Carlson, Harry W.: The Origin and Distribution of Supersonic Store Interference From Measurement of Individual Forces on Several Wing-Fuselage-Store Configurations. I.- Swept-Wing Heavy-Bomber Configuration With Large Store (Nacelle). Lift and Drag; Mach Number, 1.61. NACA RM L55A13a, 1955.

2. Thibodaux, Joseph G., Jr.: A Brief Summary of Experience in Boosting Aerodynamic Research Models. NACA RM L56E28, 1956.

3. Wallskog, Harvey A., and Hart, Roger G.: Investigation of the Drag of Blunt-Nosed Bodies of Revolution in Free Flight at Mach Numbers From 0.6 to 2.3. NACA RM L53D14a, 1953.

4. The Propulsion and Launching Section of the Guided Missile Department: The T42 Rocket Motor. Tech. Memo. No. 254, Research and Development Labs., Hughes Aircraft Co., Aug. 15, 1951.

5. Van Driest, E. R.: Turbulent Boundary Layer in Compressible Fluids. Jour. Aero. Sci., vol. 18, no. 3, Mar. 1951, pp. 145-160, 216.

6. Morrow, John D.: Measurements of the Effect of Trailing-Edge Thickness on the Zero-Lift Drag of Thin Low-Aspect-Ratio Wings. NACA TN 3550, 1955. (Supersedes NACA RM L50F25.)

7. Alford, William J., Jr.: Theoretical and Experimental Investigation of the Subsonic-Flow Fields Beneath Swept and Unswept Wings With Tables of Vortex-Induced Velocities. NACA TN 3738, 1956.

[redacted]

TABLE I

COORDINATES OF PARABOLIC FUSELAGE

[Stations measured from fuselage nose]

Station, in.	Ordinate, in.
0	0
2	.375
4	.700
6	.975
8	1.200
10	1.375
12	1.500
14	1.575
16	1.600
18	1.594
20	1.578
22	1.550
24	1.511
26	1.461
28	1.400
30	1.328
32	1.244
34	1.150
36	1.044
38	.928
40	.800

TABLE II

COORDINATES OF NACA 65A004 AIRFOIL

Station, percent chord	Ordinate, percent chord
0	0
.5	.311
.75	.378
1.25	.481
2.5	.656
5.0	.877
7.5	1.062
10	1.216
15	1.463
20	1.649
25	1.790
30	1.894
35	1.962
40	1.996
45	1.996
50	1.952
55	1.867
60	1.742
65	1.584
70	1.400
75	1.193
80	.966
85	.728
90	.490
95	.249
100	.009
L.E. radius: 0.102	

[redacted]

TABLE III

COORDINATES FOR BODY OF SMALL HUGHES FALCON MODEL

[Stations measured from body nose]

Station, in.	Ordinate, in.
0	0
.025	.079
.046	.104
.071	.122
.096	.136
.121	.146
.145	.155
.170	.161
.195	.166
.220	.170
.241	.173
.272	.176
.609	.195
.816	.198
4.508	.198
4.631	.190
4.662	.187
4.817	.173

TABLE IV

COORDINATES OF AIRFOIL FOR GROUND TESTS

[Stations measured from wing leading edge]

Station, in.	Ordinate, in.
0	0
.408	.652
.612	.788
1.025	.996
2.040	1.370
4.090	1.890
6.125	2.300
8.160	2.590
12.270	3.080
16.370	3.460

[redacted]

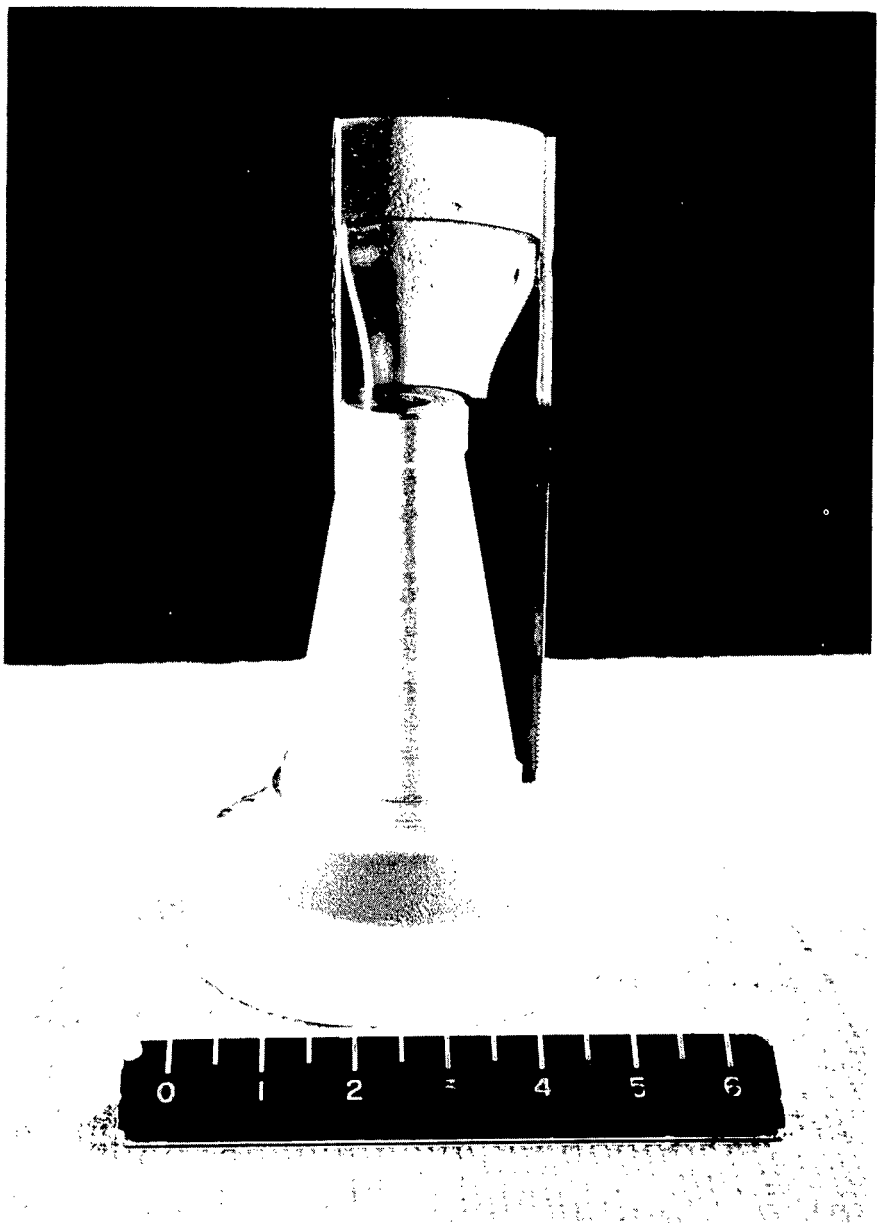

L-87695.1

Figure 1.- Photograph showing typical male launching fitting in cutaway nozzle.

[redacted]

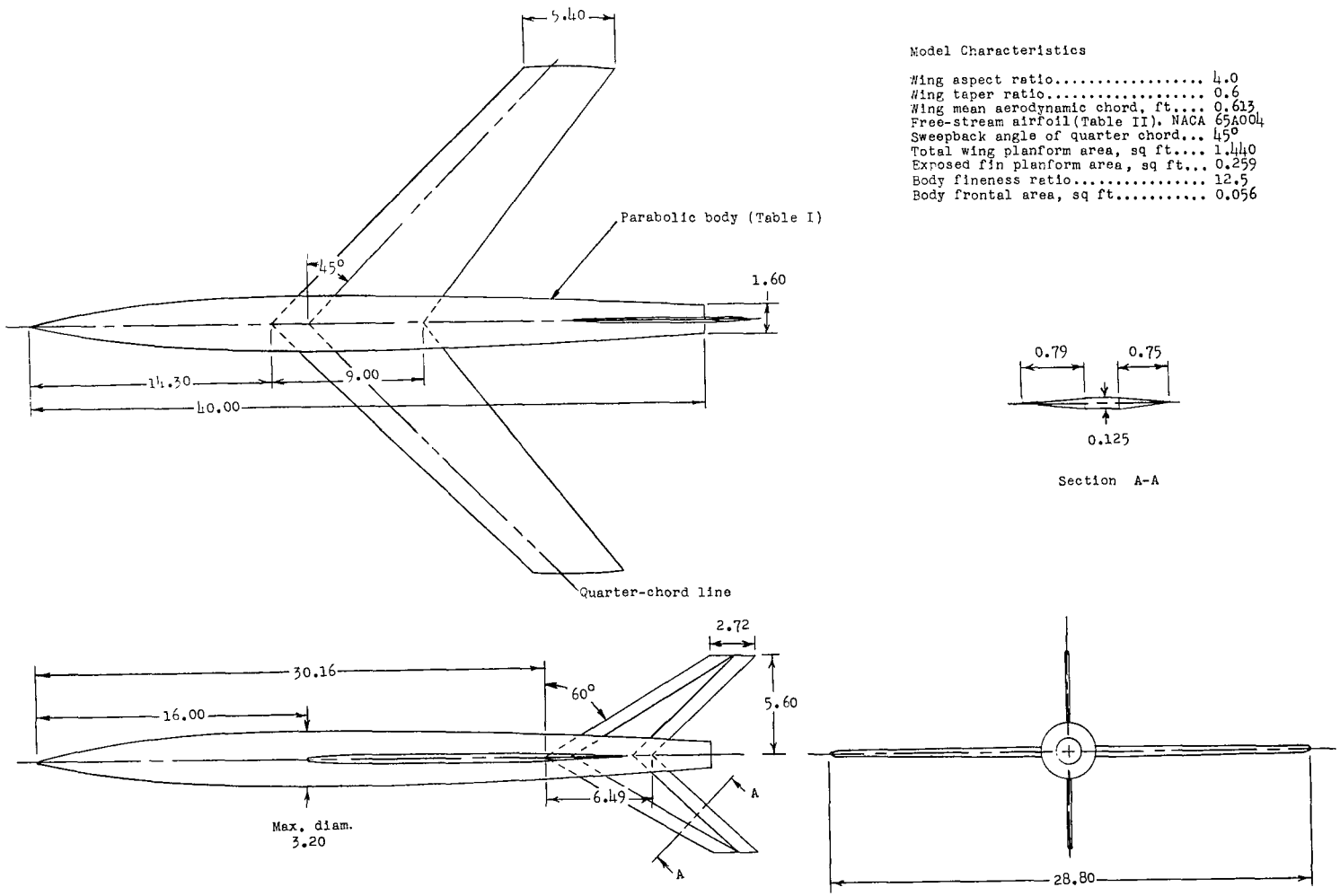

Model Characteristics

Wing aspect ratio	4.0
Wing taper ratio	0.6
Wing mean aerodynamic chord, ft	0.613
Free-stream airfoil (Table II)	NACA 65A004
Sweepback angle of quarter chord	45°
Total wing planform area, sq ft	1.440
Exposed fin planform area, sq ft	0.259
Body fineness ratio	12.5
Body frontal area, sq ft	0.056

Figure 2.- Details and dimensions of basic configuration (model A). All dimensions are in inches.

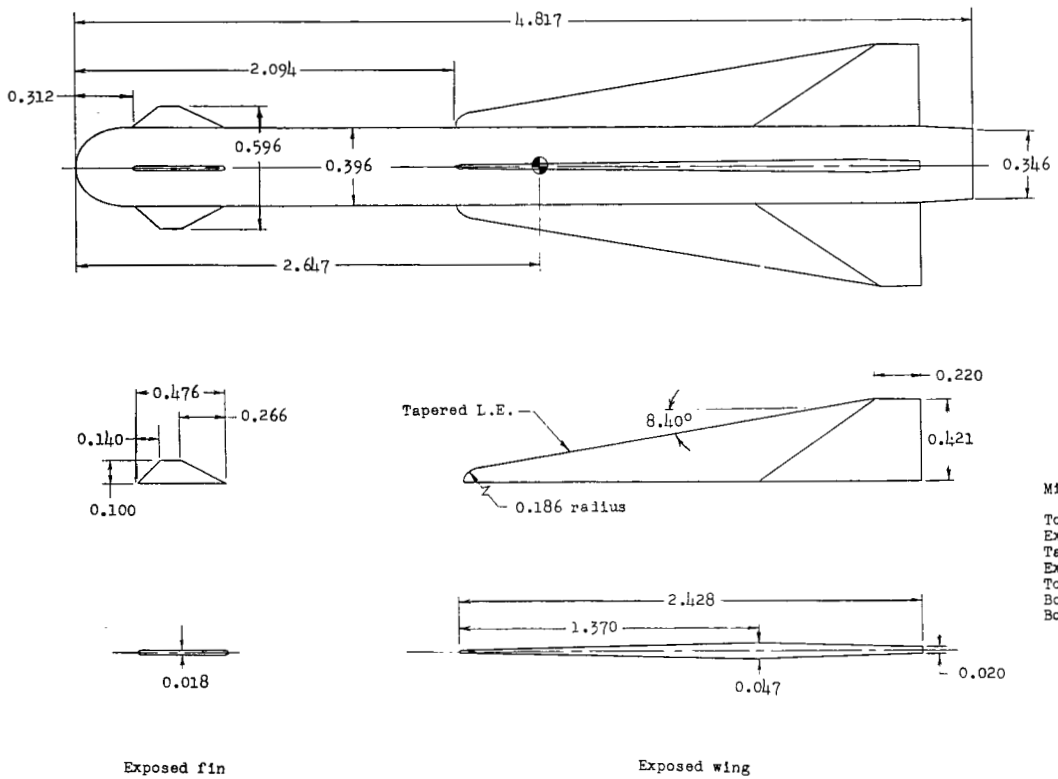

Missile Characteristics

Total exposed wing area, sq ft	0.018
Exposed aspect ratio	0.572
Taper ratio	0.091
Exposed mean aerodynamic chord, ft	0.137
Total exposed fin area, sq ft	0.00079
Body frontal area, sq ft	0.00086
Body fineness ratio	12.16

Figure 3.- Details and dimensions of small missile tested on flight models. All dimensions are in inches.

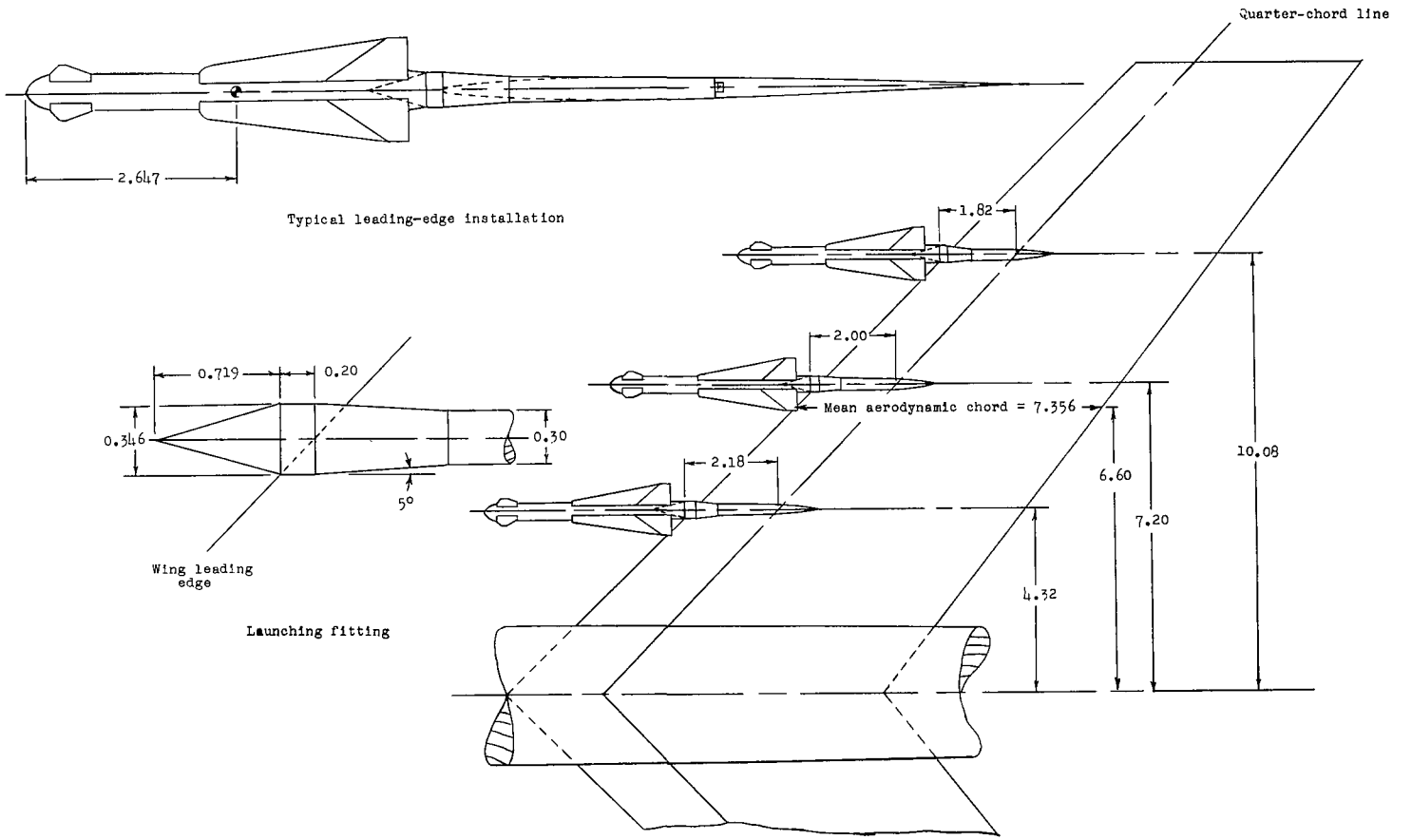

(a) Locations along wing leading edge (models B and C).

Figure 4.- Details of missile location and installation on wing. All dimensions are in inches.

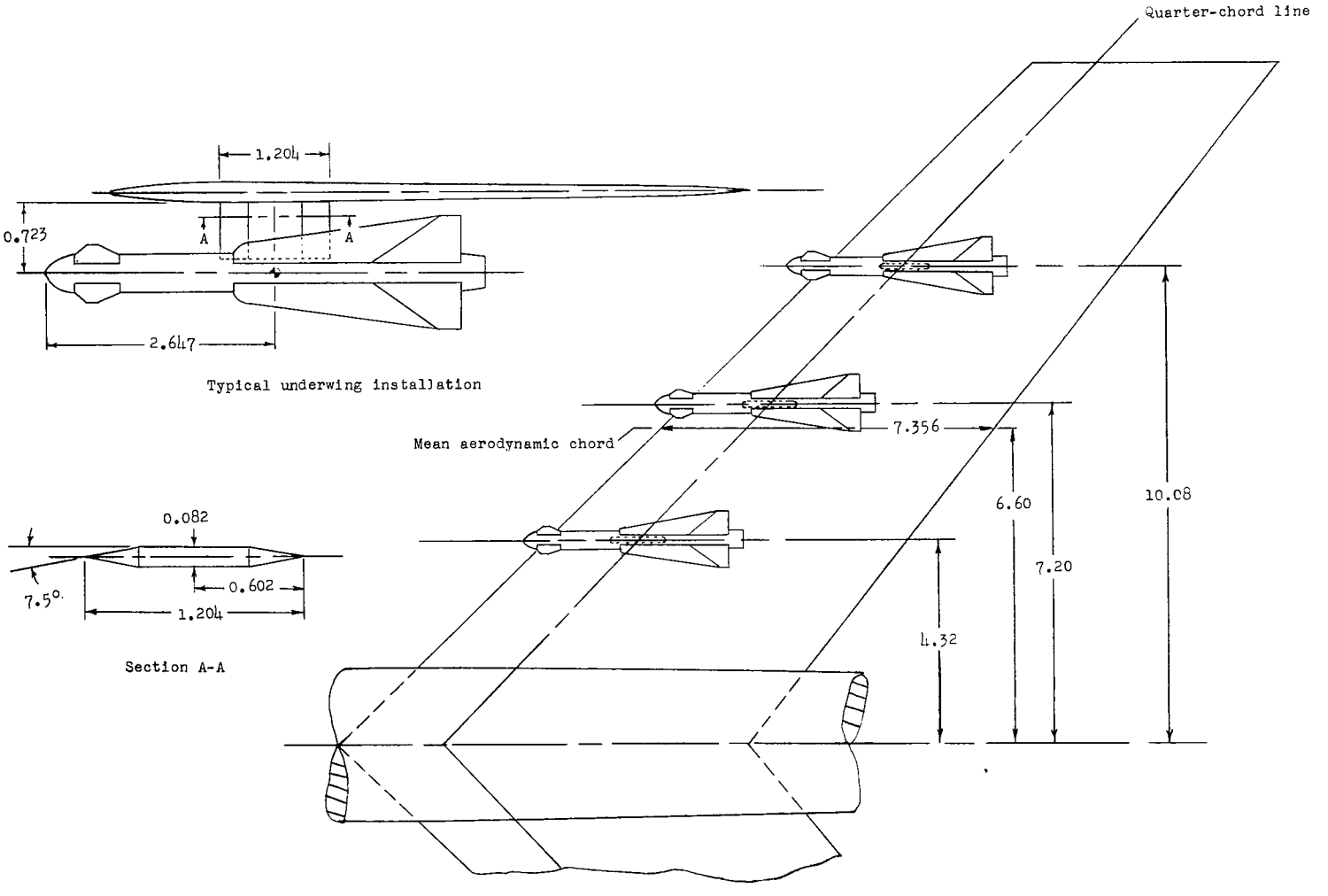

(b) Locations along wing quarter-chord line (model D).

Figure 4.- Concluded.

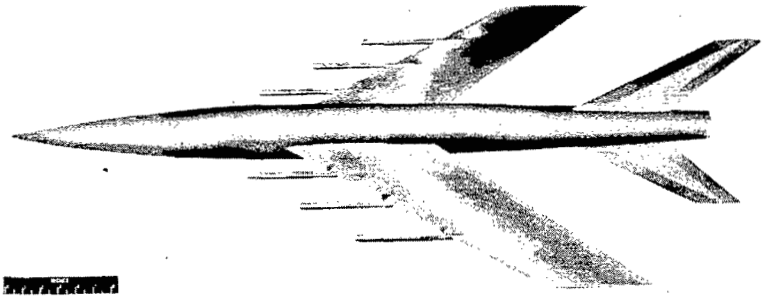

(a) Missiles mounted on wing leading edge (models B and C). L-93140.1

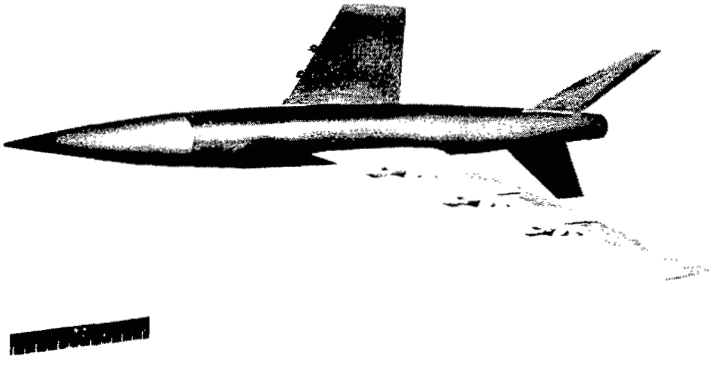

(b) Missiles mounted under the wing (model D). L-93144.1

Figure 5.- Photographs of flight models.

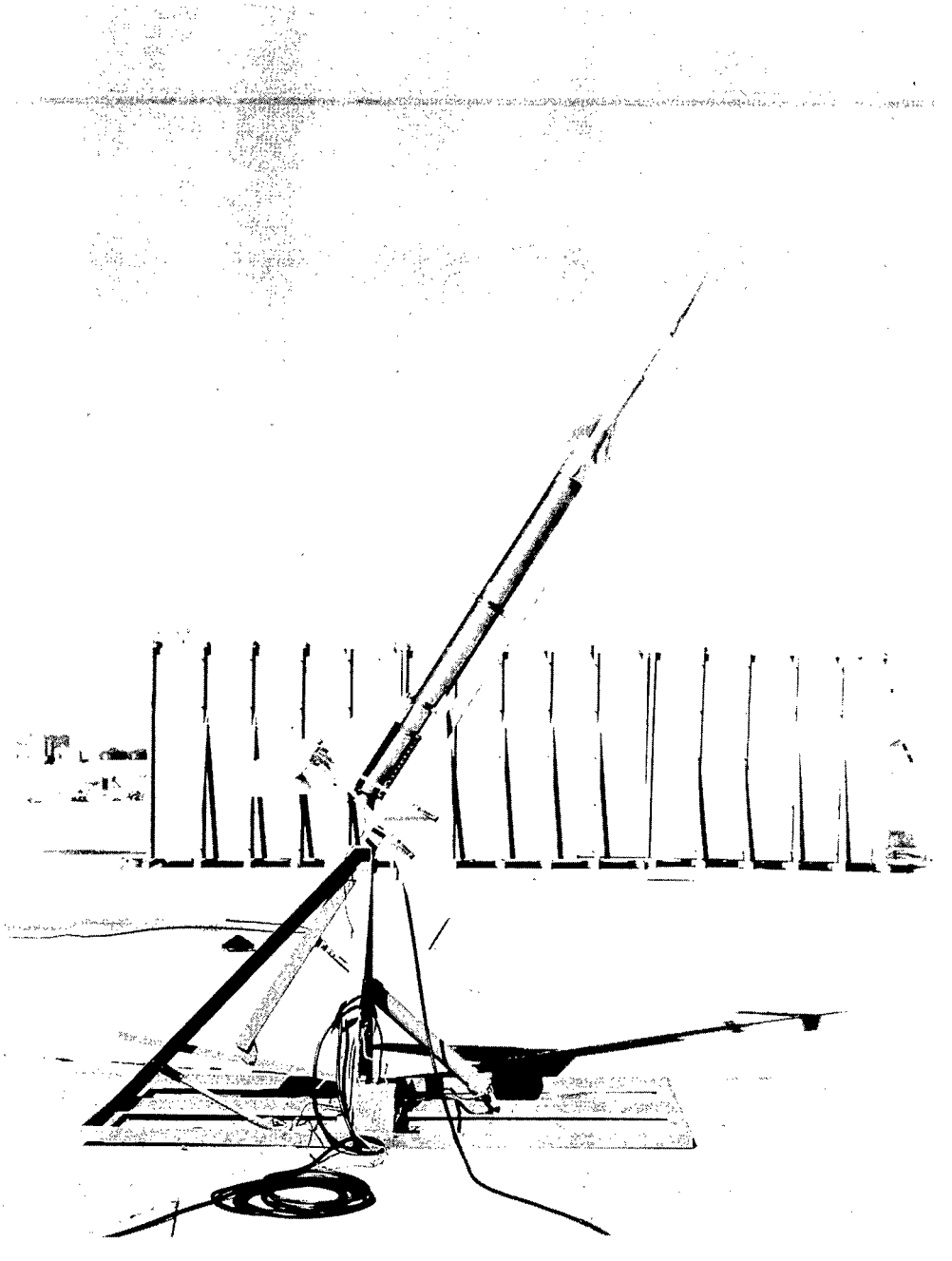

L-93766.1

(c) Model and booster on zero-length launcher.

Figure 5.- Concluded.

[redacted]

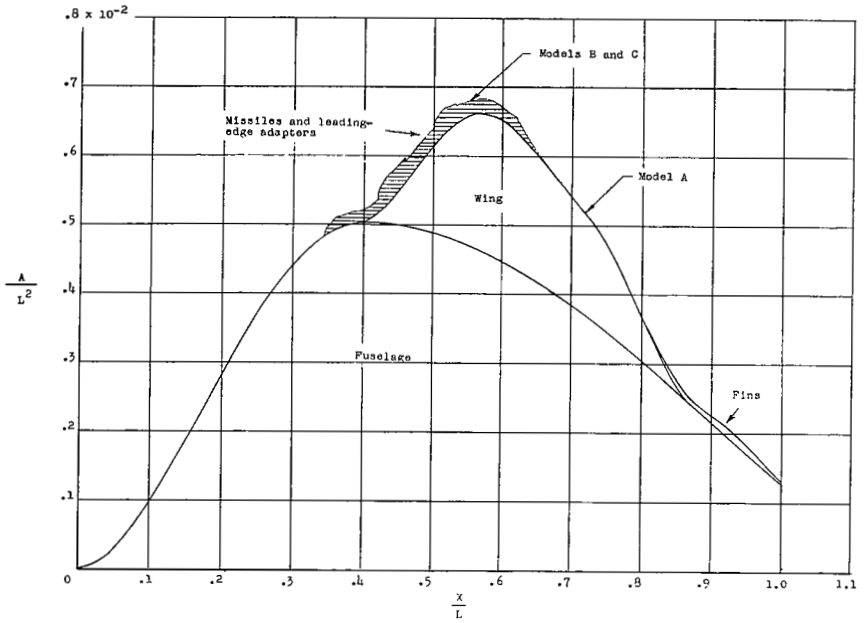

(a) Configuration with missiles along wing leading edge.

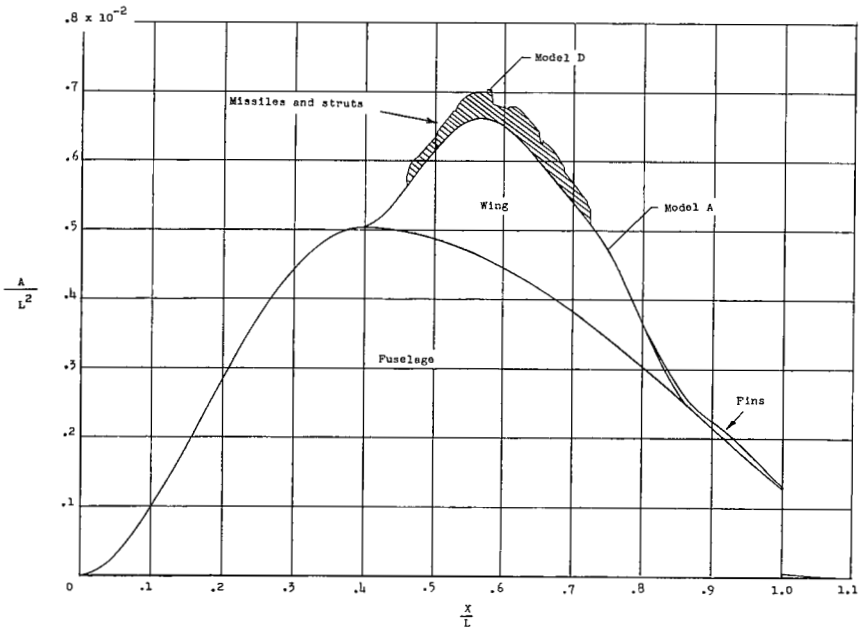

(b) Configuration with underwing missiles along quarter-chord line.

Figure 6.- Normal cross-sectional-area distributions of models tested.

[redacted]

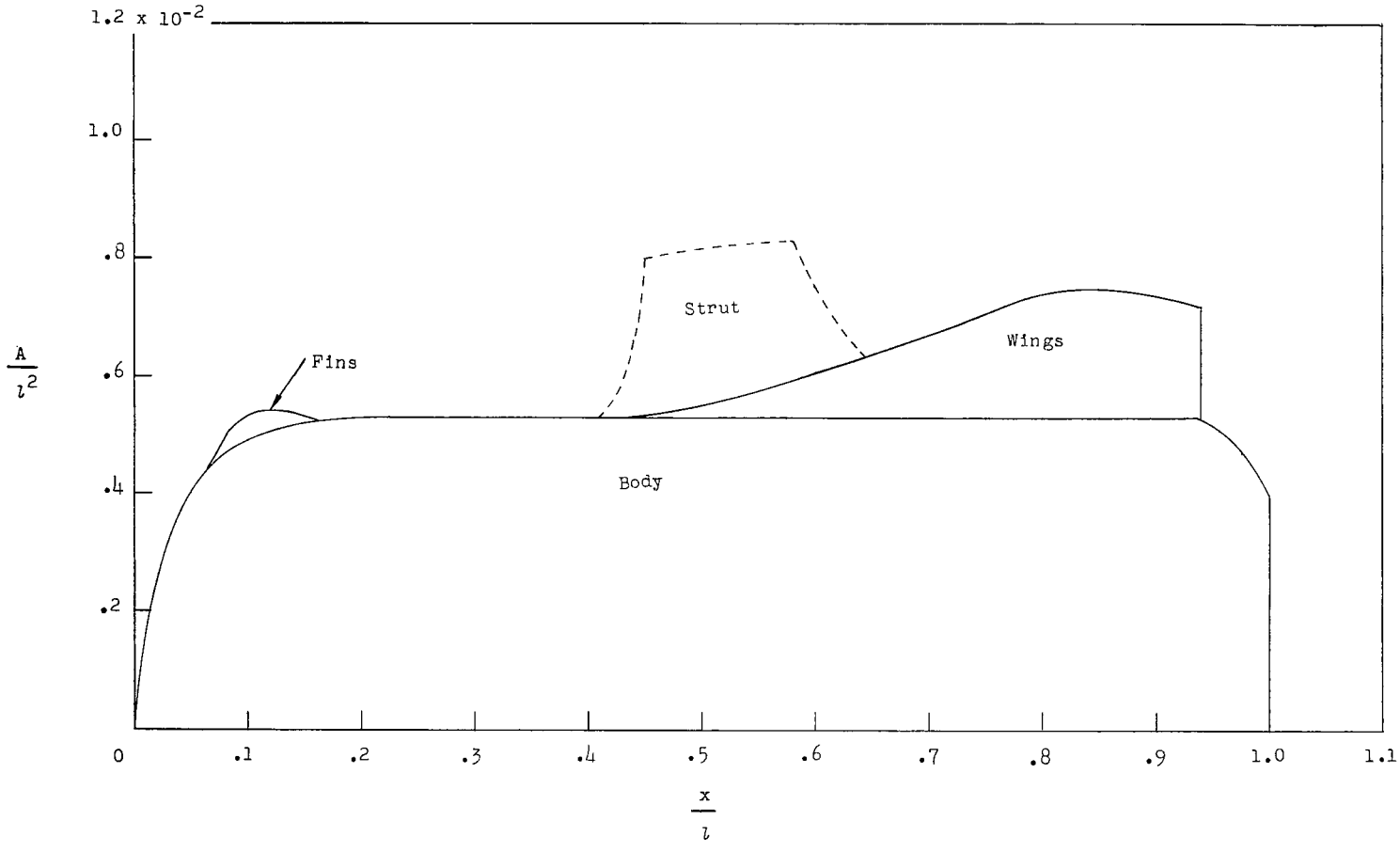

(c) Missile model.

Figure 6.- Concluded.

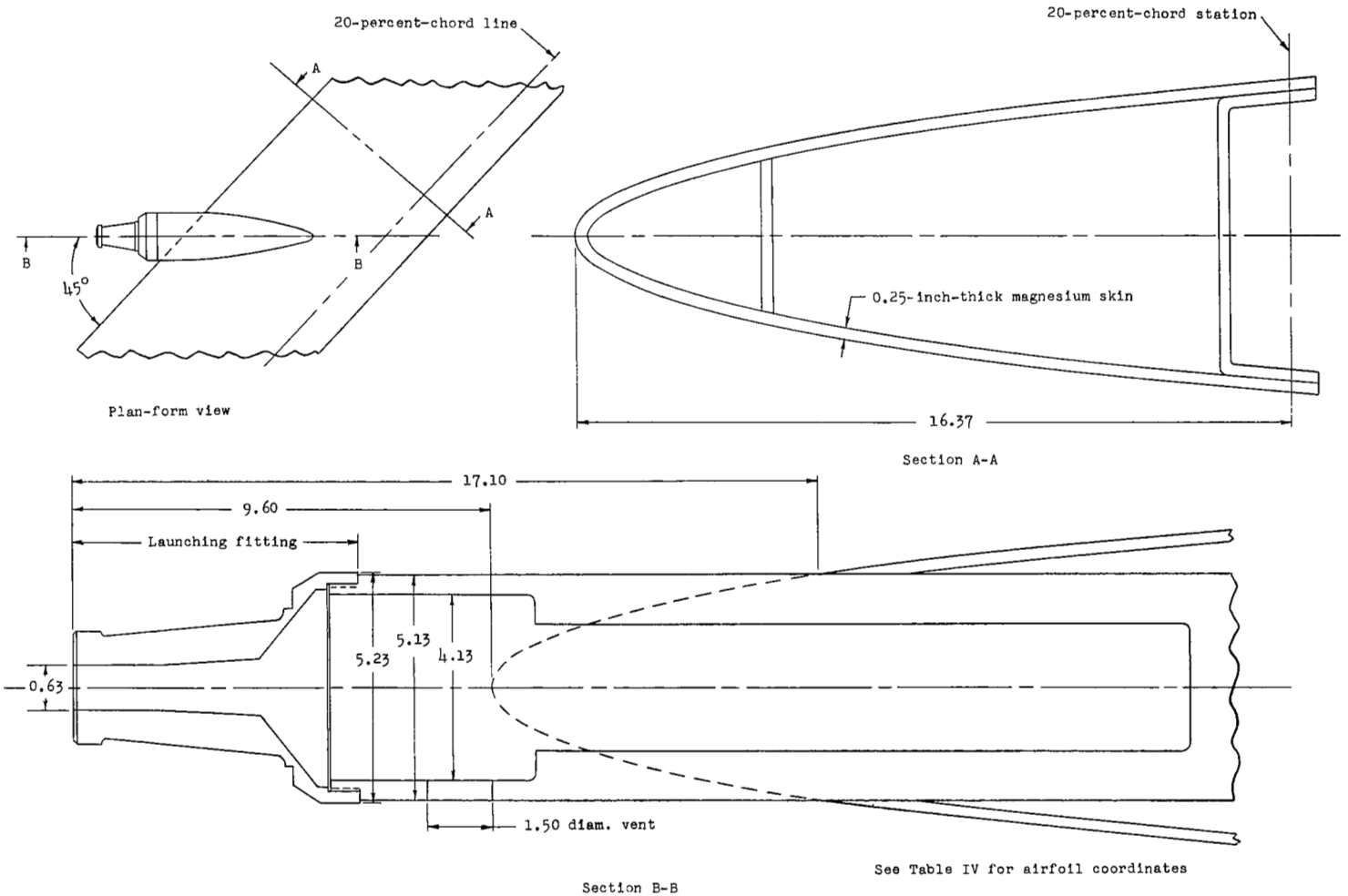

Figure 7.- General dimensions of full-scale leading-edge launcher and wing segment used for blast-damage tests. All dimensions are in inches.

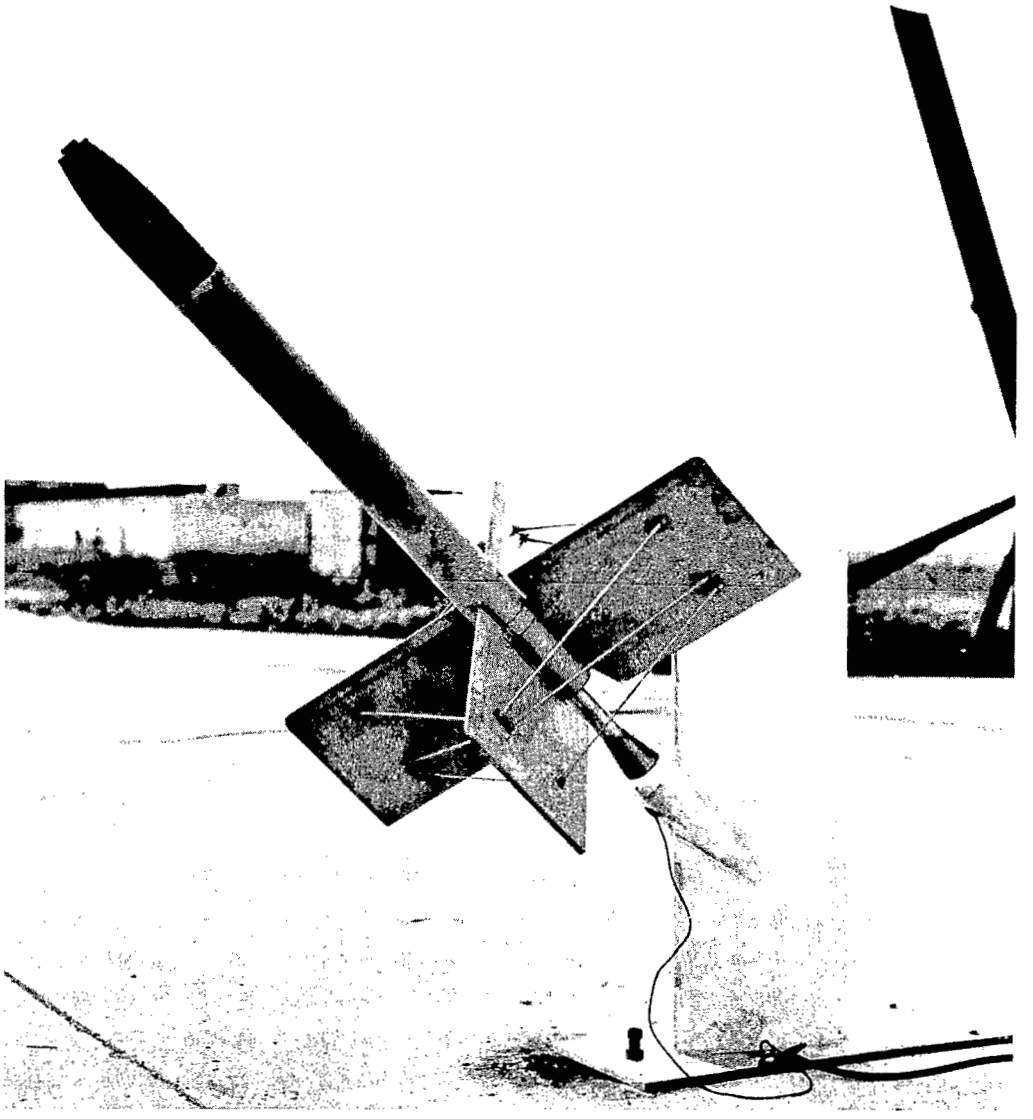

(a) General view. L-88117

Figure 8.- Photographs of full-scale wing segment, leading-edge launcher, and rocket before launching.

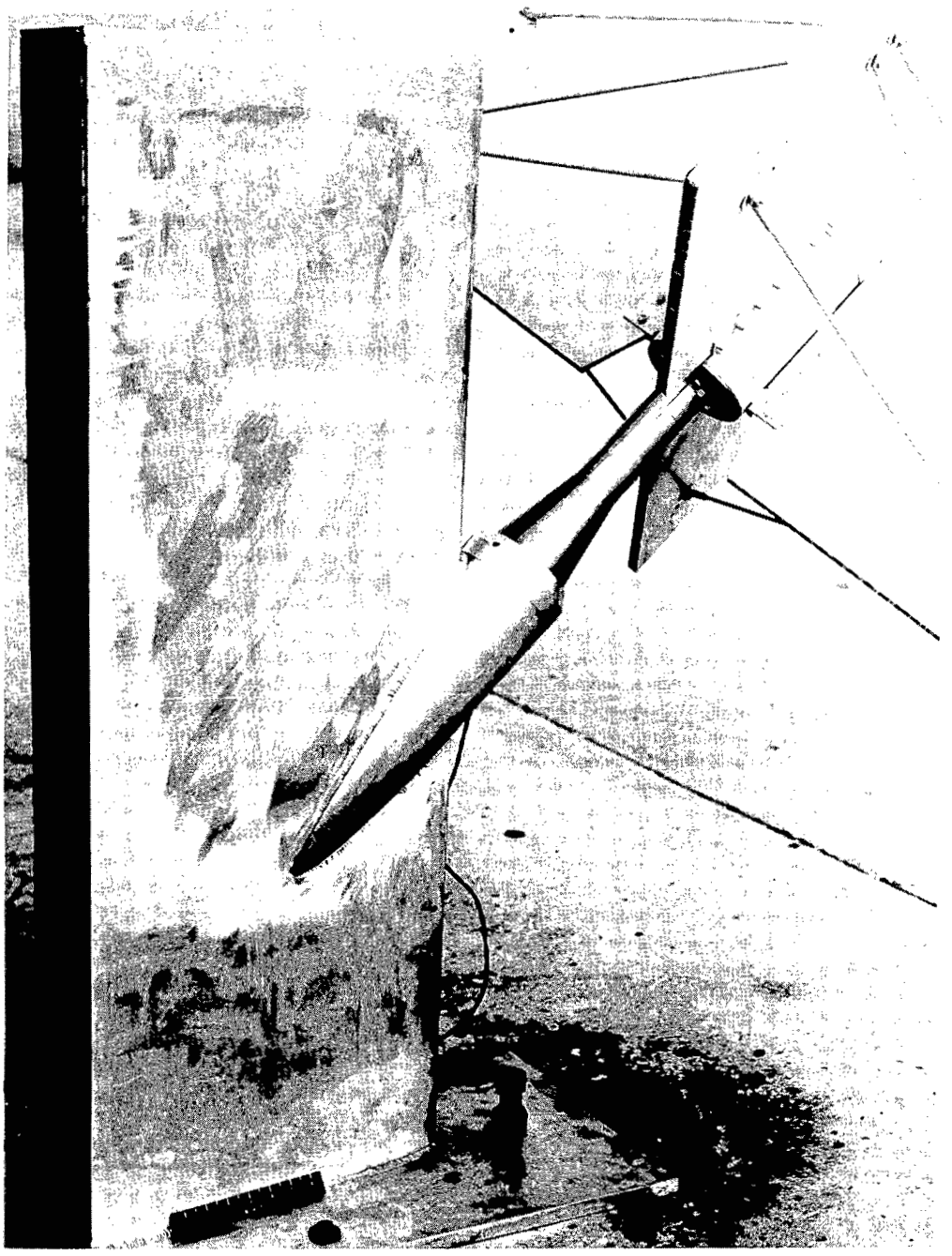

L-88119

(b) Closeup view of wing, launcher, and rocket nozzle.

Figure 8.- Concluded.

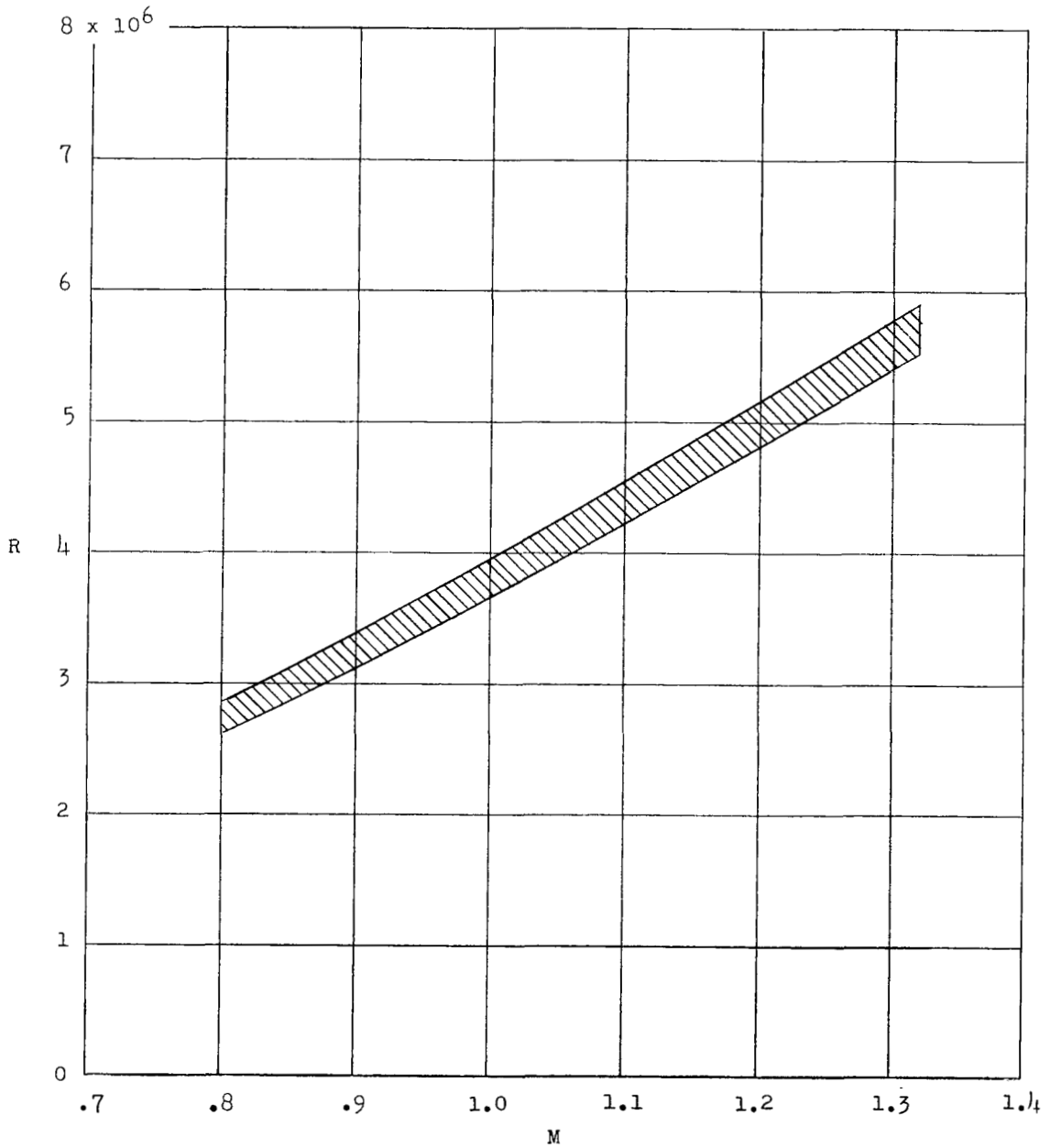

Figure 9.- Variation of Reynolds number with Mach number for flight models. Reynolds number is based on wing mean aerodynamic chord.

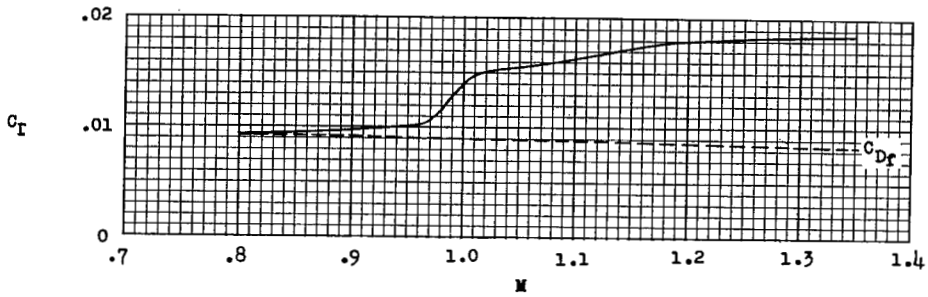

(a) Basic configuration (model A).

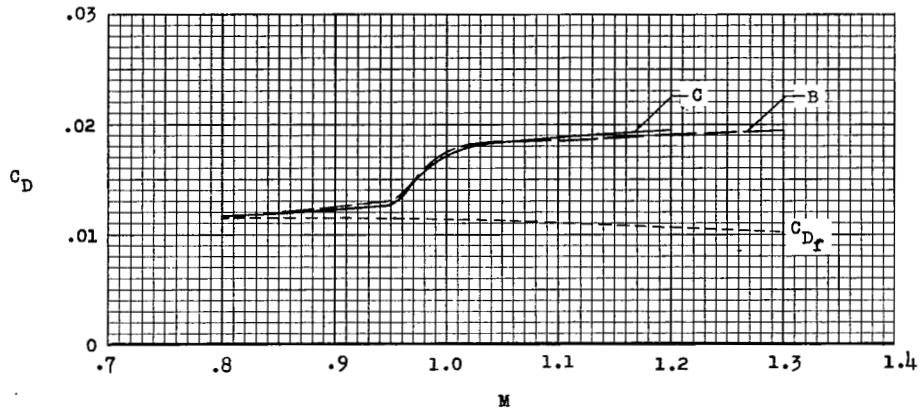

(b) Configuration with leading-edge missiles (models B and C).

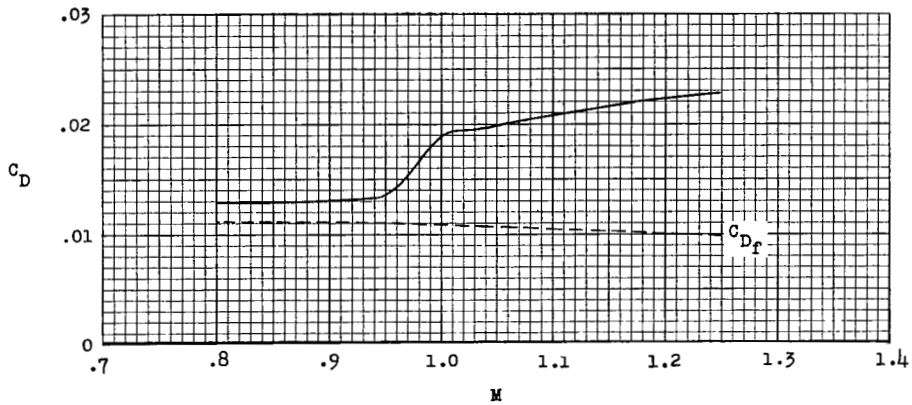

(c) Configuration with underwing missiles (model D).

Figure 10.- Variations of total drag and friction drag coefficients with Mach number for models tested.

[redacted]

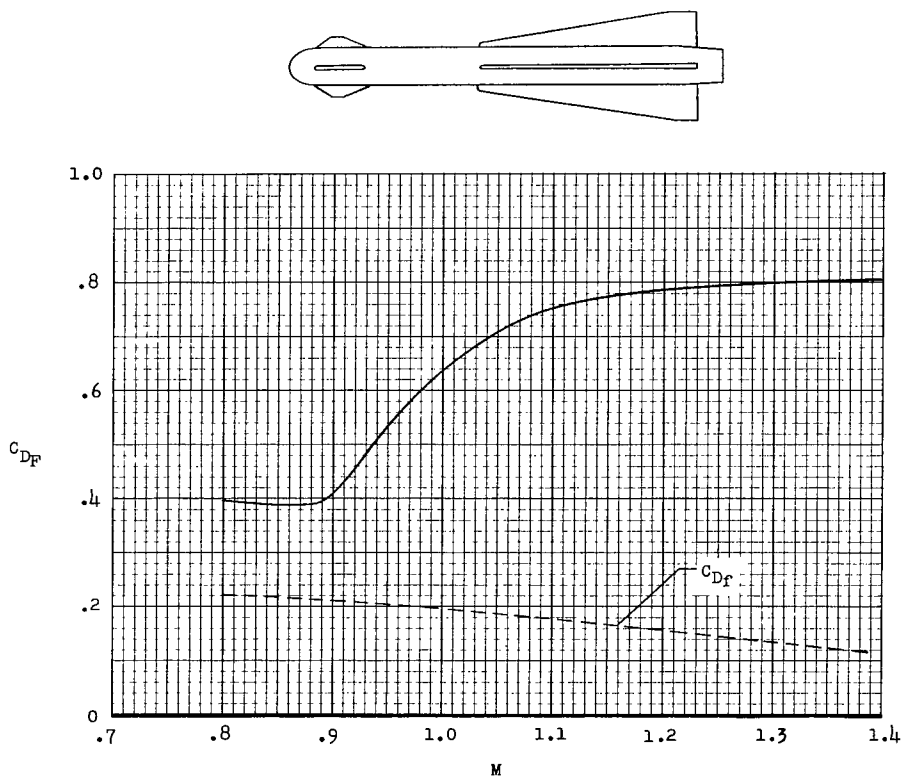

Figure 11.- Variation of missile drag coefficient (based on body maximum cross-sectional area) with Mach number.

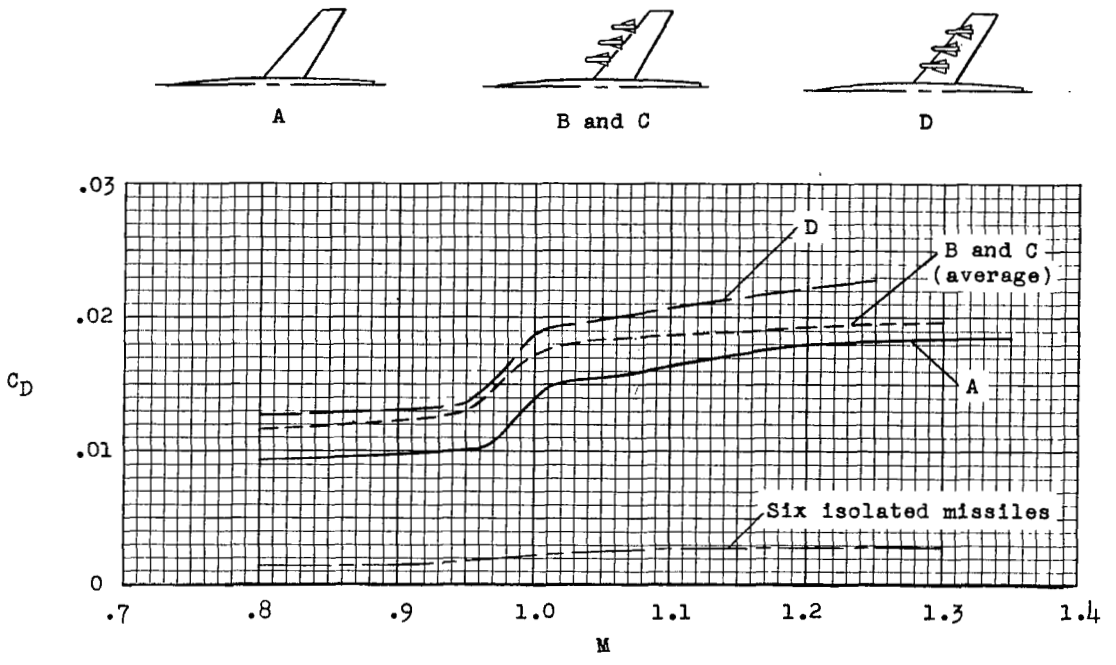

(a) Total drag.

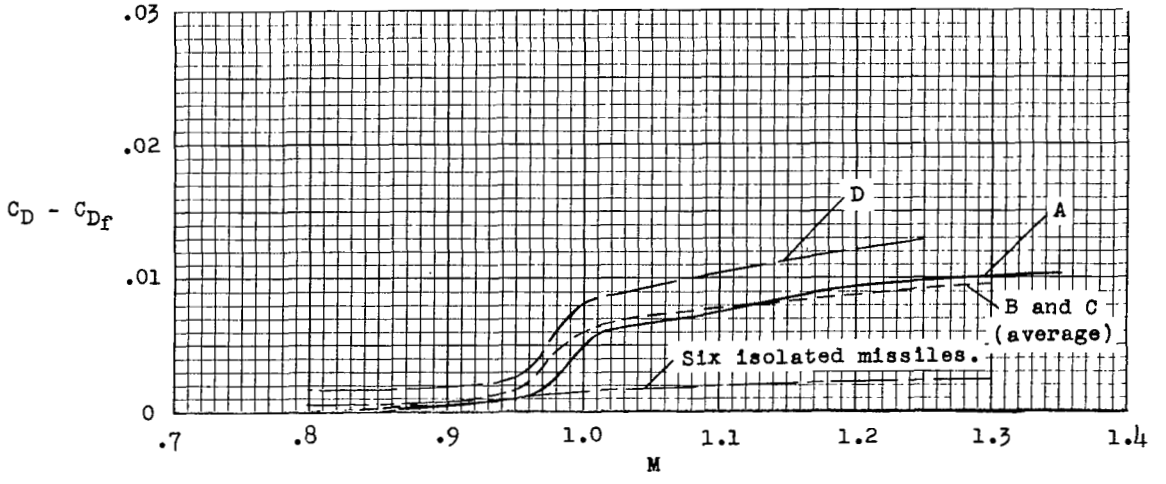

(b) Pressure drag.

Figure 12.- Comparisons of total drag and pressure drag coefficients of models tested.

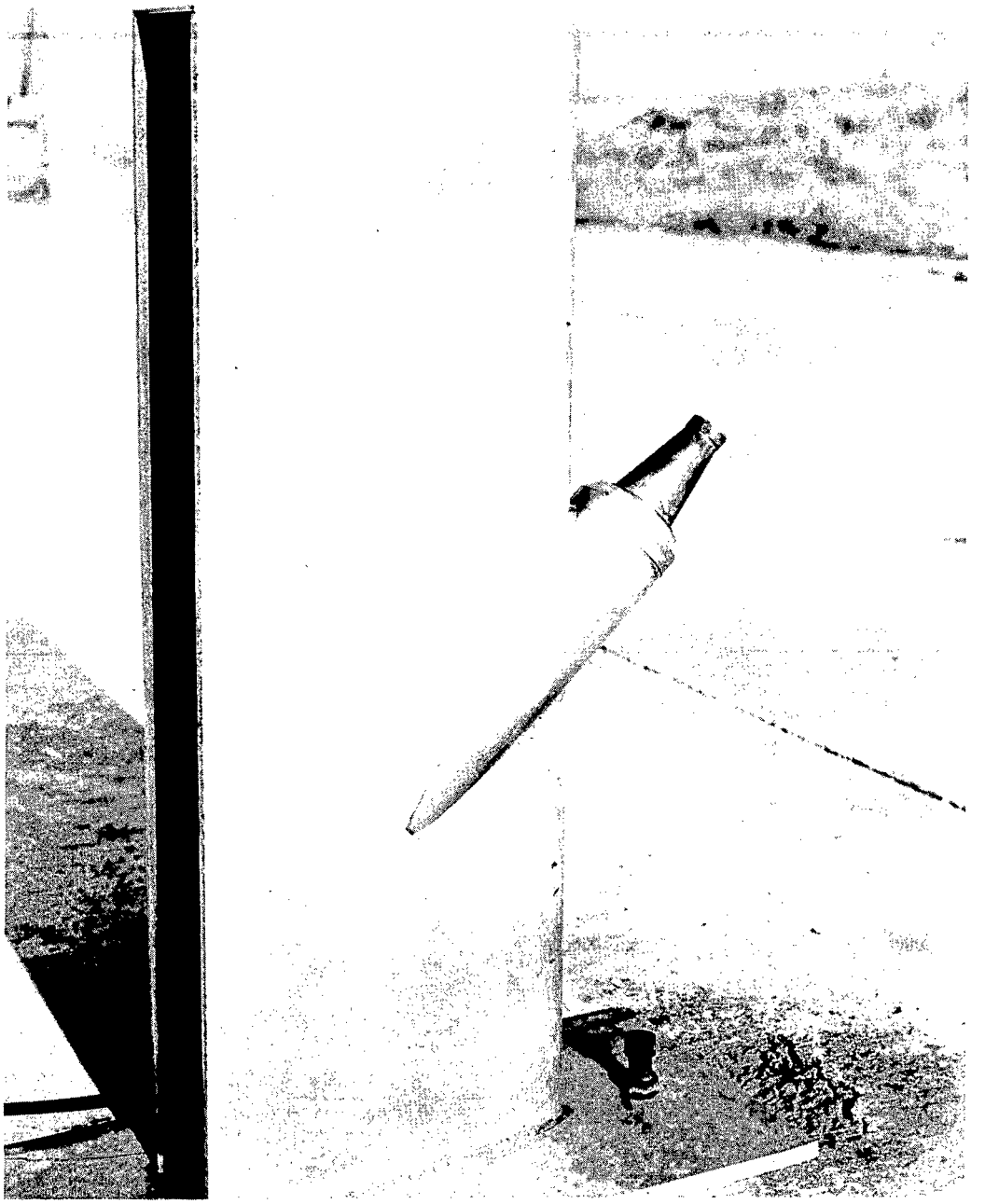

(a) General view after one firing. L-88113

Figure 13.- Photographs of wing segment and launcher after firing.

[redacted]

(b) Closeup view after one firing. L-88114

Figure 13.- Continued.

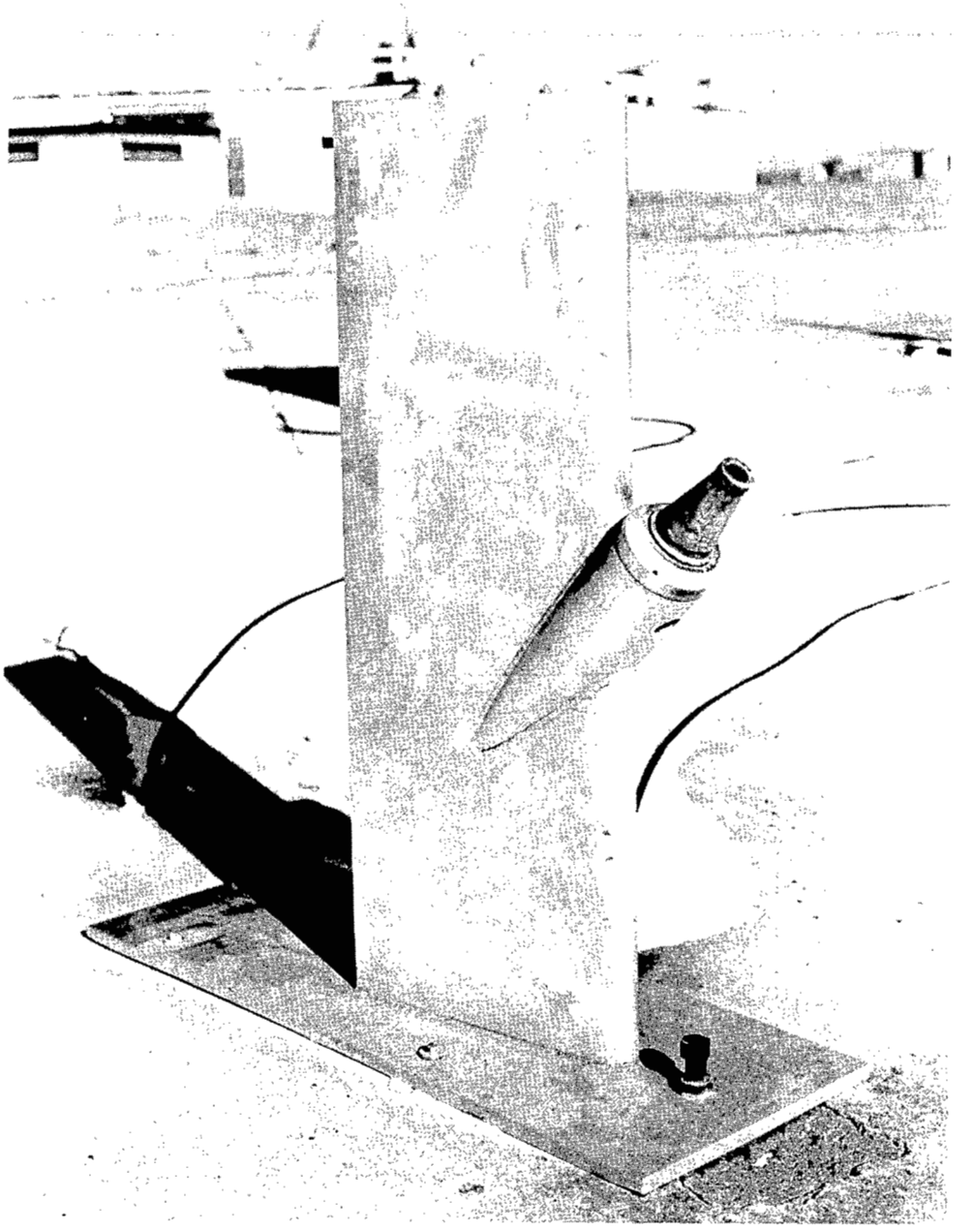

(c) General view after three firings. L-88116

Figure 13.- Concluded.

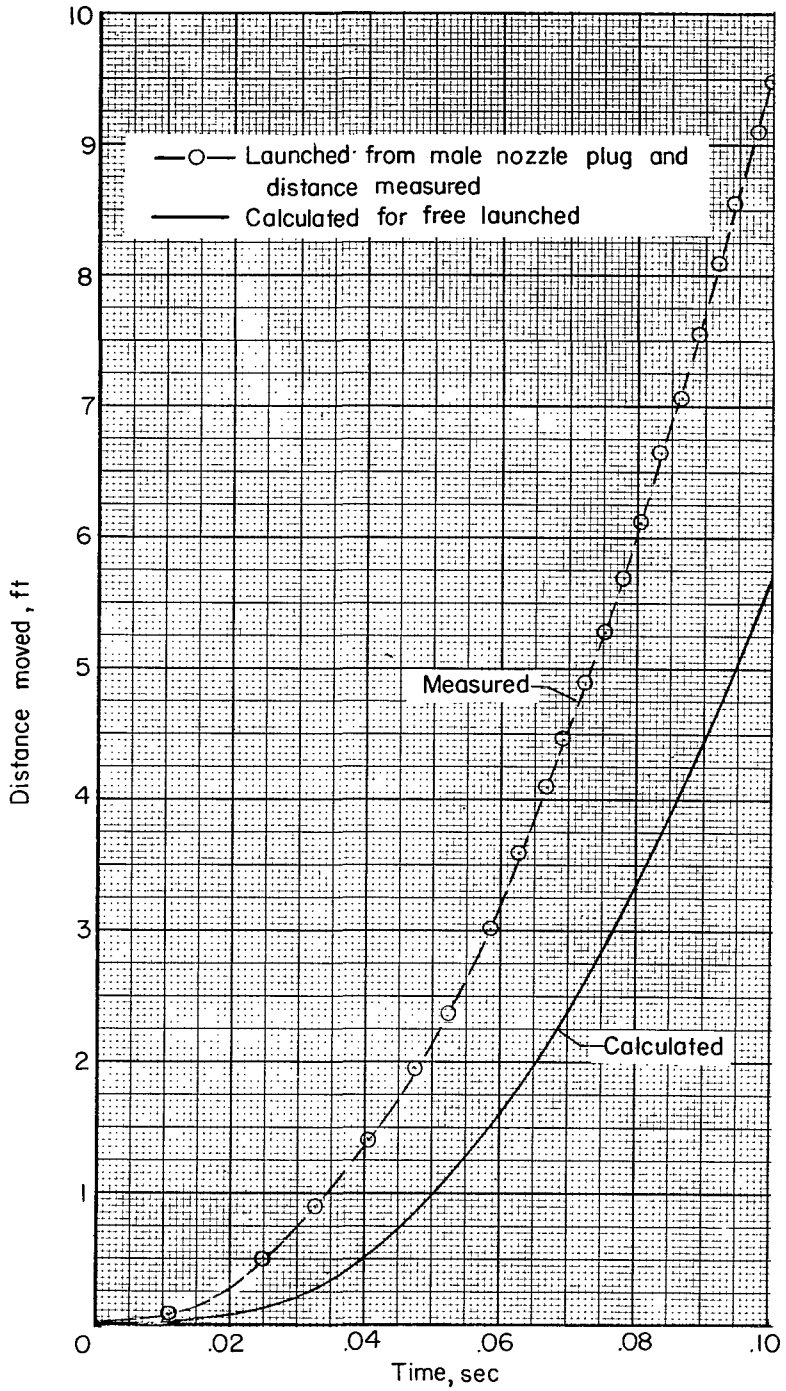

Figure 14.- Comparison of measured distance that rocket moved with blocked nozzle with the calculated distance for a free launching.

NACA - Langley Field, Va.